Low-cost and Energy-efficient RIS-based Directly Modulating Transmitter for Millimeter-wave Wideband Communications

***Abstract*—Reconfigurable Intelligent Surface (RIS)-based transmitters are a new paradigm of low-cost and energy-efficient transmitters, which circumvent the need for RF chains and only need to amplify unmodulated signals as advantages. However, current RIS-based transmitters only support discrete phase shifts, single-carrier modulation, and narrowband transmission. This letter first investigates the possibility of a RIS-based directly modulating transmitter for millimetre-wave wideband communications using an amplitude-and-phase-jointly-coding metasurface. Our proposed transmitter can realize real-valued OFDM modulation, ZF channel equalization, and 1-bit discrete beamforming while maintaining all the inherent advantages of RIS. The simulation result indicates that the proposed RIS-based transmitter performs better than the existing RIS-based single-carrier transmitter in the Rayleigh channel. Moreover, our transmitter can reach similar communications performance to its conventional counterpart with significantly lower energy consumption.**

***Index Terms*—Reconfigurable intelligent surface (RIS), direct antenna modulation (DAM), quadrature amplitude modulation (QAM), Orthogonal Frequency Division Multiplexing (OFDM).**

I. Introduction

MODERN communications demands higher working frequency bands and larger antenna arrays to address the spectrum shortage issues and to facilitate the use of multi-antenna techniques. However, conventional transmitter architecture proves to be unsuitable for massive antenna arrays, as it necessitates many RF chains for up-conversion and amplification, which can be costly and inefficient.

Reconfigurable Intelligent Surfaces (RIS) provide an effective solution to this problem. These ultra-thin, artificial surfaces are integrated with tunable elements that can dynamically manipulate the EM aspects of electromagnetic (EM) waves, such as their amplitudes, phases, and polarization [1]. Given the capabilities, RIS allows signal processing and modulation to occur via the reflection process in the air, rather than at the conventional baseband [2]. A RIS-based transmitter normally comprises of a signal source, a RIS, and its control baseband, as depicted in Figure 1(b). The signal source produces an unmodulated carrier signal, subsequently reflected by the RIS. During the reflection process, RIS directly loads the information onto the reflected signal by dynamically adjusting its tunable elements.

RIS-based transmitters have significant advantages of hardware complexity and energy efficiency. As a passive device, RIS has virtually negligible energy consumption. Only a single-frequency unmodulated signal needs to be amplified at the source, that allows the power amplifiers (PAs) to work at narrowband at their non-linear region, significantly increasing the overall power efficiency (PE). Modern PAs (normally class AB) are usually working at linear region with 30%-40% PE to avoid peak-to-average-ratio (PAPR) problems. RIS-based transmitters only amplify unmodulated signals, hence avoiding PAPR problems and allowing to use the class-E PAs, which can work at the non-linear region with theoretically maximum PE of 90%. Therefore, RIS-based transmitter can theoretically halve the energy cost and has a double PE than their conventional counterparts. Moreover, RIS-based transmitters circumvent the need of RF chains, such as the mixers, filters, and intermediate PAs in Fig. 1(a). This reduces the thermal noise and eliminates the need for more costly and complex hardware.

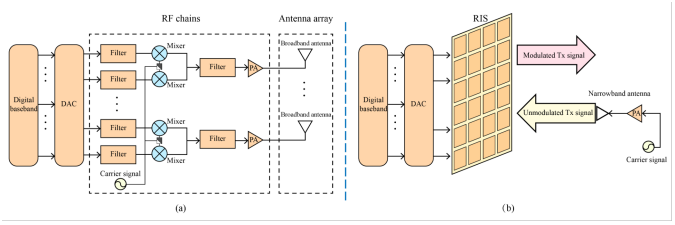

Fig. 1. Transmitter architecture (a) the conventional wireless transmitter architecture (b) the RIS-based wireless transmitter architecture.

Nevertheless, current RIS-based transmitters are still less functional than conventional transmitters, as the generated waveform highly depends on the performance of the RIS, such as its degree of freedom and accuracy. The most recently published paper on RIS-based transmitters all aimed to replicate the functionality of conventional transmitters, such as their modulation schemes and multi-antenna techniques, when maintaining the inherent advantages of RIS.

The paper [3] and [4] proposed a RIS-based binary frequency shift-keying (BFSK) and quadrature phase shift keying (QPSK) transmitter, respectively. The paper [5] further proposed an elaborately designed RIS, which achieved a 360-degree phase coverage, enabling an 8-phase shift keying (8PSK) wireless communications prototype. This year, paper [6] and [7] proposed a non-linear approach for RIS-based quadrature amplitude modulation (QAM) and a novel transmitter concept for discrete phase shifts, respectively. In addition, many existing multi-antenna techniques have been successfully implemented in RIS-based transmitters, such as MIMO [2], beamforming [8], beam steering [9], and non-linear/dual polarization [10].

Nevertheless, to the best of the authors' knowledge, current RIS-based transmitters only support discrete phase shifts, single-carrier modulation, and narrowband transmission. The paper [6] realized 256QAM using a non-linear approach by manipulating the time delay and duty ratio of the control signal. However, their methodology induces serious spectrum pollution, which implies the difficulty to derive wideband modulation.

Against the background, this letter first investigates the possibility of a RIS-based directly modulating transmitter for wideband communications, particularly at a millimetre-wave band. Inspired by [11], our work first implements an amplitude-and-phase jointly coding metasurface in the transmitter design. The reflection amplitudes of the RIS can vary in a continuous domain from 0.1 to 0.9 when the reflection phases can be inversed independently. The RIS provides an additional degree of freedom to our transmitter against the earlier works. In addition, Hermitian Symmetric is applied in our transmitter for obtaining real-valued OFDM, which can be generated through arbitrary amplitude modulation. Moreover, we introduce the equalization and 1-bit discrete beamforming method of our RIS-based transmitter. In simulation, we compare the communications performance of our proposed RIS-based transmitter, the existing single-carrier RIS-based transmitters, and the conventional wideband transmitter.

The rest of this letter is organized as follows. Section II introduces our system model, including the RIS model, communications model, and baseband control signal generation. Section III presents RIS-based wireless techniques, including RIS-based modulation, channel equalization and beamforming. Section IV presents the simulation results ——comparison with RIS-based and conventional benchmarks. Section V concludes this letter.

II. System model

This section provides the system model of our RIS-based communications, including the RIS model, the communications model, and the baseband control signal generation. 1) The RIS model introduces the RIS hardware constraints and how RIS's considered and modelled in this work. 2) The communications model presents the signal propagation process from the signal source to the receiver. 3) The baseband signal generation model gives the process from information bits (10101…) to the control signal of RIS to the propagation signal (i.e., the signal reflected by RIS).

A. RIS Model

In this work, the RIS is initialized as an input-output (IO) function according to the EM aspects (i.e., S-parameters) of the RIS antenna design in paper [11]. The core problem is to find out the relationship between the external control signals and the RIS responses.

Each unit of the RIS is embedded with a PIN diode, which can be analyzed by its equivalent circuit, consisting of a variable resistor and a capacitor C=0.15 pF. The variable resistor can be further presented by the control signal, according to Shockley Equation:

$$I_D = I_s \left(e^{\frac{V}{nV_T}} - 1 \right) \tag{1}$$

$$R_D = \frac{V}{I_s \left(e^{\frac{V}{nV_T}} - 1 \right)} \tag{2}$$

where I_D is forward current, I_s is the bias voltage, n is reverse saturation current, V_T is the ideal factor, and is thermal voltage.

$$Z_{in} = \left[Z_D // \frac{1}{jwC_g} + 2jwL_p \right] // Z_0 \tan\left(\beta_s d_s\right) / \varepsilon_r \tag{3}$$

Given the equivalent circuit of the RIS unit, the input impedance of the unit can be expressed as:

where $Z_D = R_D // C$, d_s is the thickness of the substrate. β_s and β_0 are the propagation constants in the dielectric substrate and air, respectively. C_g , L_p, and ε_r are three unknown constants. The reflection coefficient of a RIS unit can be thereby obtained:

$$\Gamma_n = \frac{Z_{in} - Z_0}{Z_{in} + Z_0} = A_n e^{j\varphi_n} \tag{4}$$

where Z_0 is the characteristic impedance in space. A_n and φ_n are the amplitude and phase reflection coefficients of the n-th unit, respectively.

Given Equation (1) to (4), the input impedance Z_{in} and the reflection coefficient Γ_n are only determined by Z_D, where Z_D is only determined by the control signal (i.e., the external voltage).

Despite the unknown constants in Equation (3), the one-to-one corresponding relationship between the control signal and the reflection coefficients Γ_n can be obtained by statistics and curve fitting. Therefore, in the following, we only take the reflection coefficient into consideration. The exhaustive sets of all possible reflection coefficients $\Gamma_n = A_n e^{j\varphi_n}$ for our RIS are

$$A_n \in [0.1,\ 0.9], \forall n \tag{5}$$

$$\varphi_n \in \{0,\ \ \pi\}, \forall n \tag{6}$$

which is equivalent to

$$0.1 \leq |\Gamma_n| \leq 0.9,\ \forall n \tag{7}$$

For simplicity without losing generality, the reflection coefficients are normalized and subject to

$$|\Gamma_n| \leq 1,\ \forall n \tag{8}$$

Moreover, the respond speed of the used PIN diodes T_{PIN}= 0.038 us . The updating frequency of the unit thereby subject to

$$f_n \leq 26\ MHz,\ \forall n \tag{9}$$

Above all, the RIS is modelled as an IO function from control signals to reflection coefficients, whose output is an arbitrary real-valued signal, subject to Equation (8) and (9).

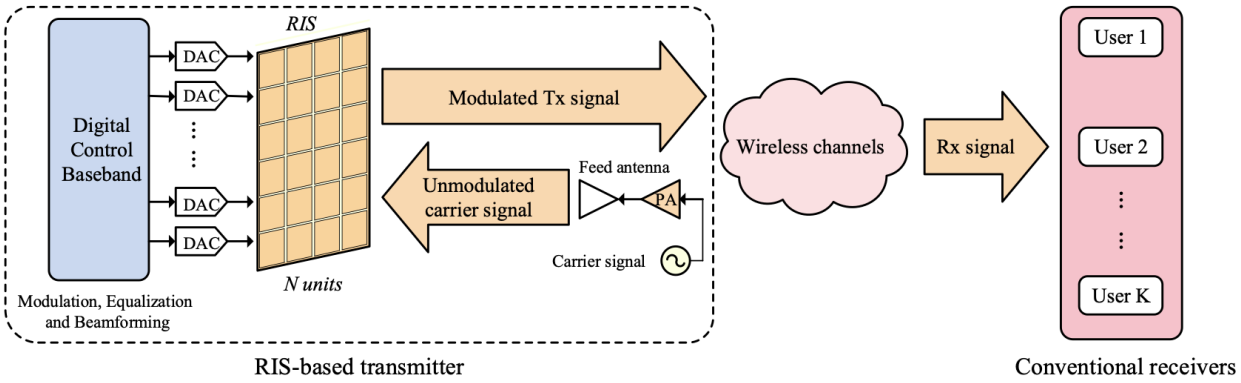

Fig. 2. RIS-based communications system, including our RIS-based transmitter, wireless channel, and conventional receivers.

B. Communications Model

We consider a downlink multi-user communications scenario to reveal the advantages of overcoming multi-path and frequency-selective fading and implementation of orthogonal frequency division multiple access (OFDMA), as shown in Fig. 2. Each user is allocated to a 15 kHz subcarrier. The number of users is set the same as the number of subcarriers. The RIS-based transmitter comprises a single-frequency signal source, the RIS and its control baseband. The RIS is a uniform planar array (UPA) placed near the signal source and far from the receiver. The signal source generates the signal, then reflected by RIS and propagated to the receiver via the wireless channel. The modulation, equalization, and beamforming directly happen at the reflection process in the air. The propagation of the signal from the signal source to the receiver is as follows.

The signal source provides a single-frequency planar signal, as the carrier

$$s\left(t\right)=\sqrt{P}e^{2\pi f_c t} \tag{10}$$

where f_c is the carrier frequency, and P is the transmit power of the signal source. Since the RIS-based transmitter circumvents thermal noise caused by RF chains, we assume that the addictive white Gaussian noise (AWGN) induced by the transmitter is negligible. The transmitted signal $s(t)$ is then emitted to the cascaded channel h from the signal source to the RIS to the receiver, $i.e.$,

$$h={h_{Tx\_RIS}}^{H}\Omega_{RIS}h_{RIS\_Rx} \tag{11}$$

where $H_{Tx\_RIS}\in\mathbb{C}^N$ is the channel from the signal source to the RIS, $h_{RIS\_Rx}\in\mathbb{C}^N$ is the channel from the RIS to the receiver,N is the total number of RIS units, and Ω_{RIS} is a diagonal matrix as

$$\Omega_{RIS}=diag\left(A_1e^{j\varphi_1},\ A_2e^{j\varphi_2},\ \ldots,A_Ne^{j\varphi_N}\ \right)\ \in\mathbb{C}^{N\times N} \tag{12}$$

where $A_Ne^{j\varphi_N}$ is the reflection coefficient of the n-th unit of the RIS. The reflection coefficient can be further expressed as

$$\Omega_{RIS}=\Omega_A\bigodot\Omega_\varphi \tag{13}$$

where $\Omega_A=diag(A_1,A_2,...,A_N)\in\mathbb{C}^{N\times N}$ is the amplitude reflection coefficient, $\Omega_\varphi=diag(e^{j??\varphi_1},e^{j\varphi_2},...,e^{j\varphi_N})\in\mathbb{C}^{N\times N}$ is the phase reflection coefficient, and $\bigodot$ is the Hadamard product.

The path loss between the signal source and the RIS is too small to be negligible due to the short distance. The phase change from the signal source to the receiver is avoidable by properly placing the signal source and the RIS. Therefore, h_{Tx_RIS} is herein set as an identity matrix. We assume the communications happen with dense obstacles, suffering from multi-path fast fading. The channel matrix can be modelled as an independent and identically distributed (i.i.d.) Rayleigh fading channel as

$$h_{RIS\_Rx}=\sqrt{\mu d^{-\alpha}}\ \left[|a_1|\,e^{\beta_1},|a_2|\,e^{\beta_2},\ldots,\ |a_N|\,e^{\beta_N}\right] \tag{14}$$

where d is the distance between the RIS and the receiver, α is the pass loss exponent, and μ is the path loss at the reference distance of 1 meter (m). The entries are i.i.d. complex Gaussian random variables with zero mean and unit variance, i.e., . $|a_N|e^{\beta_N}\sim CN(0,1)$ The received signal $r(t)$ is thereby

$$r\left(t\right)=hs\left(t\right)+w\left(t\right) \tag{15}$$

where $w(t)$ is AWGN, induced by the receiver, $w(t)\sim CN(0,\sigma^2)$. We assume that K users are active in the communications system, and each user is allocated to a 15kHz subcarrier. The signal received by the k-th user can be expressed as

$$r_k\left(t\right)=h\sqrt{p_k}s_k\left(t\right)+h\sum_{i\neq k}\sqrt{p_i}s_i+\ w_k\left(t\right) \tag{16}$$

where p_k denotes the transmitted power allocated for the K-th user/subcarrier, which satisfies the following constraints

$$p_k>0,\forall k,\sum_{i=1}^{K}p_i\leq P \tag{17}$$

Specially, the power allocated to different users/subcarriers (i.e.,p_i) is determined by the RIS rather than the signal source. The signal to noise (SNR) for the k-th user can be expressed as

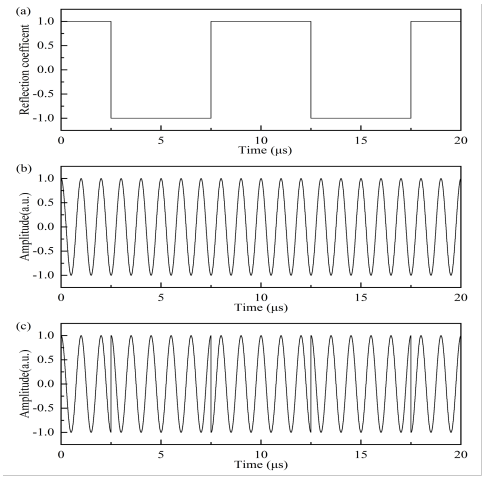

Fig. 3. RIS-based BPSK Modulation. (a) The time-varying reflection coefficient between 1 and -1, (b) The carrier signal $s(t) = e^{2\pi f_c t}$, (c) The reflected signal $s_{RIS}(t) = \Omega_{RIS} s(t)$. .

$$SNR_k = \frac{p_k |H_k|^2}{p_i \sum_{i \neq k} |H_i|^2 + \sigma_k{}^2} \tag{18}$$

where $H = w.h$ is the frequency-domain channel matrix, and W is the Fast Fourier Transform (FFT) matrix. The capability of the k-th user is given by

$$C_k = \log_2 (1 + SNR_k) \tag{19}$$

and the capability of the system can be given by

$$C_{sum} = \sum_{i=1}^{K} \log_2 (1 + SNR_i) \tag{20}$$

C. Signal Generation Model

This section gives the baseband signal generation of the RIS control signal, represented by the reflection coefficient in this work. We first review the conventional baseband generation. In the conventional transmitter, the bit stream first goes through a channel encoder and then is modulated to a digital baseband signal. After digital-to-analogue conversion (DAC), the analogue baseband signal goes through amplification and up-conversion to be the Tx signal and propagation.

In RIS-based transmitter, the first two steps are unaltered. The bit stream goes through a channel encoder and modulates to a digital baseband signal. However, the digitally modulated baseband signal is then converted to the digital control signal of the RIS rather than output as an analogue baseband via DAC. Each complex sample of the digital modulated signal represents an amplitude and phase value corresponding to a complex reflection coefficient. The mapping relationship between the reflection coefficients and the control signal is given by Equation (1) to (4). Therefore, given the digitally modulated baseband signal, the digital control signal can be obtained. The digital control signal then goes through DAC to load on the RIS to obtain the corresponding reflection coefficient. The reflected signal is given by

$$s_{RIS}(t) = \Omega_{RIS}\ s(t) \tag{21}$$

which is the modulated carrier signal. In particular, many existing research quantize and convert the samples of the digital control signal to a binary number, which allows the RIS to be controlled by a digital coding sequence (0101…).

Since channel coding and channel estimation are irrelevant to the achievement of RIS-based transmission, our system doesn't consider them. For simplicity, we assume that the channel distribution information (CDI) and channel state information (CSI) are ideally obtained. To enhance the system performance, we adopt a Zero-forcing (ZF) algorithm to our RIS-based transmitter for channel equalization with 1-bit discrete phase beamforming. The channel equalization and beamforming will be discussed later.

III. RIS-BASED MODULATION, EQUALIZATION AND BEAMFORMING

This section presents the wireless techniques of our RIS-based transmitter, including RIS-based direct modulation, equalization, and beamforming.

A. RIS-based Modulation

This section starts with a RIS-based directly modulating BPSK example. Then, we propose an equivalent model, which considers the RIS as a mixer. Given the equivalent model, our RIS is sufficient for generating an arbitrary real-valued signal, but OFDM samples are normally complex values. Finally, we introduce how to obtain a real-valued OFDM baseband signal.

1) RIS-based BPSK Modulation

To make the abstract concept clear, we herein first give the simplest RIS-based modulation example. Given the Equation (4), (14) and (21), the received signal is given by

$$r(t) = \frac{\sqrt{P\mu d^{-\alpha}}}{N} \sum_{n=1}^{N} A_n |a_n| e^{j\varphi_n - \beta_n - 2\pi f_c t} + w\ (t) \tag{22}$$

For simplicity, we assume that P =1, and each unit of the RIS modulates the same information onto the carrier. The power is equally allocated to all subcarriers, and the channel equalization perfectly eliminates the Raleigh fading. The AWGN is eliminated at receiver. Therefore, the Equation (22) becomes

$$r(t) = \sqrt{P\mu d^{-\alpha}} A(t) e^{j\varphi(t)} \tag{23}$$

where each unit of the RIS has the same reflection coefficient at the same time. For BPSK modulation, the RIS only needs to switch between two different phase shifts, subject to

$$A_n(t) e^{j\varphi_n(t)} \in \left\{e^{j0}, e^{j\pi}\right\} = \{1, -1\},\ \forall n,\ t \tag{24}$$

A time-domain RIS-based BPSK modulation is given in Fig. 3. The time-varying reflection coefficient is shown in Fig. 3(a).

The carrier signal is shown in Fig. 3(b). According to Equation (21), the signal reflected by RIS is given by Fig. 3(c), which is a BPSK signal.

Given Equation (21) and Fig. 3, the reflected signal is essentially the product of the reflection coefficient and the carrier signal. RIS serves as an equivalent mixer, which mixes the reflection coefficient and the carrier signal. Meanwhile, the reflection coefficient serves as the equivalent baseband modulated signal.

2) RIS-based OFDM Modulation

The basic OFDM signal generation process is given as follow. 1) A bit stream first goes through channel encoder. 2) Then, the bit stream completes serial-parallel conversion and is allocated to different parallels/subcarriers for modulation. 3) Aftermodulation, the subcarriers are summed up by inverse fast Fourier transform (IFFT). 4) The IFFT output does parallel-to-serial conversion and is added with cyclic prefix for overcoming multi-path fading. 5) Output as a time-domain OFDM signal.

Since the reflection coefficient serves as the equivalent baseband modulated signal of the RIS-based transmitter, if we can shape the reflection coefficient to an OFDM signal in time, we will realize RIS-based OFDM modulation. To the best of the author's knowledge, no existing RIS can generate arbitrary complex signals over broadband with acceptable control speed. Instead, our RIS-based transmitter can generate an arbitrary real-valued signal, subject to the Equation (8).

Moreover, given the principle of Hermitian Symmetric, we can obtain a real-valued OFDM signal by using additional spectrum resources. We assume that there are K subcarriers and the step (4) is a K-points IFFT (fully loaded). The Hermitian Symmetric is "imposed" on the symbols of the k-th subcarrier by ensuring that

$$x_0 \ = x_{\frac{K}{2}} \in \mathcal{R} \tag{25a}$$

$$x_k \ = x^*_{K-k}, \ \forall k \in \left(0, \frac{K}{2}\right) \tag{25b}$$

where x_k is the k-th IFFT input, and normally x_0=0 to avoid DC bias.

The discrete OFDM signal is a sequence of OFDM samples from a complex set in the complex signal space. The key process is the IFFT, which obtains the summation of all subcarriers. The Hermitian Symmetric ensures that the IFFT inputs are all complex conjugate pairs. Therefore, the summation of $\frac{K}{2}$ conjugate pairs is obviously real-valued.

As discussed in the system model, each subcarrier of our wideband signal is allocated with 15kHz.The sampling rate of multi-carrier modulation depends on the number of subcarriers and the sampling rate of each subcarrier. Given Equation (9), our RIS-based OFDM communications have a maximum symbol rate of $\frac{26MHz}{15KkHz}$., which limits our maximum number of IFFT numbers to 1024.

B. RIS-based Channel Equalization and beamforming

Besides RIS-based modulation, our transmitter can also implement channel equalization and beamforming for better communications performance without additional hardware or energy consumption. When RIS-based modulation, we consider all units of the RIS to be controlled by the same control signal, as they modulate the same information onto the carrier. Differently, RIS-based channel equalization and beamforming consider all units of the RIS as independent antennas suffering from independent wireless channels. We herein adopt the ZF algorithm and 1-bit discrete beamforming at the transmitter side, given perfect CSI, and subject to our RIS's constraints.

The optimal reflection coefficient of n-th unit can be formulated as

$$\tilde{\Gamma}_n = A_n {A'}_n e^{j\varphi_n - {\varphi'}_n} \tag{26}$$

where $A_n e^{j\Psi_n}$ is the modulation coefficient, and $A_n e^{j\Psi_n}$ is the equalization and beamforming coefficient. The optimal reflection coefficient matrix is thereby

$$\tilde{\Omega}_{RIS} = diag\left(\tilde{\Gamma}_1, \tilde{\Gamma}_2, \ \ldots, \tilde{\Gamma}_n\right) \tag{27}$$

Due to the RIS's hardware constraints caused by antenna design, RIS typically only has discrete phase shifts, equally distributed in the phase domain $[0, 2\pi)$.To minimize the quantization error,

$$\hat{\varphi}'_n = \arg\min |\varphi'_n - \tilde{\varphi}'_n| \tag{28}$$

And the ${A'}_n$ and ${\varphi'}_n$ of the optimal reflection coefficient are obtained by

$${A'}_n, {\varphi'}_n = \arg\max \left| tr\left(\tilde{\Omega}_{RIS} h_{RIS\_Rx}\right)\right| \tag{29}$$

In particular, our RIS-based transmitter only loads information onto amplitudes, and the beamforming factor can only inverse the amplitude value to plus or minus. Therefore, given perfect CSI (i.e., all parameters in Equation (14) are known), a low computational complexity method is given by

$$\hat{A}'_n = \ \arg\min |{A'}_n - \ |a_n|| \tag{30a}$$

$$\text{s.t.} \ \ A_n {A'}_n \leq 1 \tag{30b}$$

$$\varphi_n = \begin{cases} \pi, & \beta_n - \ \pi \geq 0 \\ 0, & \beta_n - \ \pi < 0 \end{cases} \tag{31}$$

As the CSI is perfectly known, A'_n should be the closest number to $|a_n|$ under the constraint of Equation (8). The 1-bit discrete phase shift beamforming can only adjust the amplitude value to be plus or minus. Therefore, we adjust all complex samples to plus real-valued samples to obtain the maximum BER-SNR performance.

IV. Results & Evaluation

This section gives our simulation results to validate the performance of our proposed RIS-based wideband transmitter design. We compare the SNR-BER performance of our RIS-based wideband transmitter with the existing RIS-based high-order QAM single-carrier transmitter and the conventional

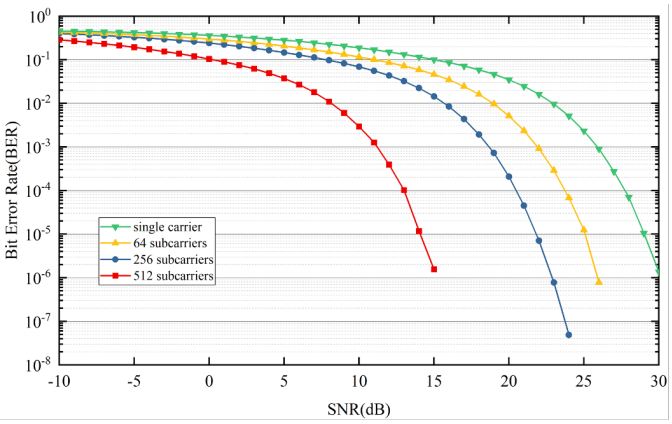

Fig. 4. BER performance versus SNR for RIS-based real-valued OFDM/complex QAM when the transmit power of signal source P=10 dBm, the number of subcarriers is varying from 1 to 512, and the modulation scheme is 256QAM.

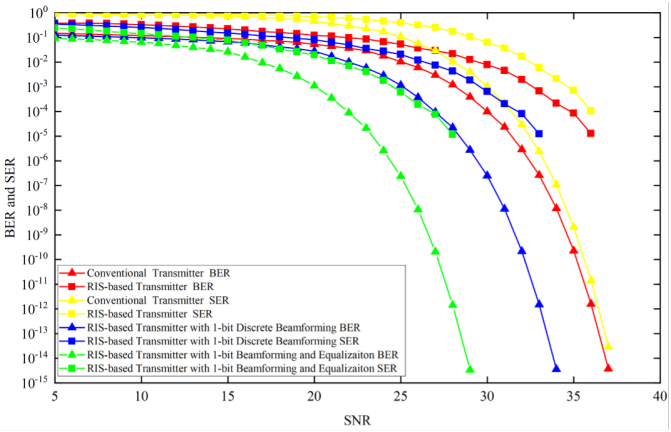

Fig. 5. BER and SER performance versus SNR for RIS-based real-valued OFDM and conventional complex OFDM when the transmit power of signal source P=10 dBm, the modulation scheme is 256QAM, and the number of FFT-points is 256.

complex OFDM transmitter. The path loss and at the reference distance of 1 m, the path loss exponent for the channel from the RIS to the users, and the average noise power are set as $\mu = -20$ dB, $\mathfrak{a} = 2.8$ and $\sigma^2 = -70$ dBm, respectively, consistent with the settings in [12]. The distance between the RIS and the Rx is set as 1 m. The number of RIS units is set as 64. The carrier signal is set as 10GHz within the working frequency of our RIS. Since OFDMA is adopted, we assume each user is allocated to a 15kHz subcarrier. The total number of subcarriers/users should be no more than 1024 to meet the Equation (9).

On the transmitter side, we generate a data stream with 40000 random bits for transmission. The data stream is reshaped by serial-to-parallel conversion and firstly modulated with 256-QAM modulation at each IFFT input (i.e., subcarrier). After adding cyclic prefix and real-valued IFFT, a conventional real-valued OFDM baseband signal is obtained. Each OFDM sample then generates a corresponding reflection coefficient. The time-varying reflection coefficient is mixed with the carrier signal to simulate the RIS reflection process. On the receiver side, the demodulation is conventional.

Fig. 4 compares the SNR-BER performance of our RIS-based transmitter and the existing most advanced single-carrier modulation RIS-based transmitter in paper [], where the subcarriers/users of ours. Even without beamforming and Equalization, our RIS-based real-valued OFDM transmitter still performs better than the single-carrier RIS-based transmitter. The ideal transmission speed of single-carrier and multi-carrier modulation without pilot symbols and cyclic prefixes is the same. Both single-carrier and multi-carrier modulation can theoretically reach the Shannon Limit. The difference is that multi-carrier modulation has better antijamming capability against multi-path and frequency-selective fading against fast-fading models. Moreover, the existing RIS-based transmitter single-carrier modulation will seriously pollute the surrounding spectrum resource due to the coupled reflection phases and amplitudes. 15kHz is not sufficient for RIS-based single-carrier modulation to adopt FDM.

Fig. 5 compares the SNR/SER-BER performance of our RIS-based transmitter and its conventional counterpart. Specifically, our RIS-based transmitter is a RIS-aided single narrowband antenna, where the antenna transmits an unmodulated carrier signal. The conventional counterpart is a single wideband antenna, where the antenna directly transmits the modulated OFDM signal. Our RIS-based real-valued OFDM transmitter has a slightly lower SNR/SER performance than its conventional counterpart due to a normalization loss of $\log 10\left(0.9^2\right) \approx 0.9$ dB. After Equalization and beamforming, our RIS-based transmitter has better BER performance against the conventional one for around 7 dB. We herein consider the CSI to be perfectly known. Therefore, ZF equalization almost removes the channel influence according to Equation (30), except for the AWGN induced by the receiver. Even with the 1-bit beamforming, our RIS-based transmitter still has better SNR/BER performance than the conventional transmitter without RIS.

Meanwhile, our RIS-based transmitter has significantly better power efficiency and energy consumption than the conventional transmitter. Our RIS-based transmitter only needs a narrowband antenna to transmit an unmodulated signal, where the PA can work at its non-linear region, and the PE will be over 70%. However, the conventional transmitter needs a wideband antenna to transmit a modulated wideband signal, where the PA needs to work at its linear region, and the PE will be only around 40%. Therefore, our RIS-based transmitter almost halves the power consumption with better BER-SNR performance.

V. Conclusions

In this letter, we first propose a low-cost and energy-efficient RIS-based wideband transmitter design using an amplitude-and-phase-jointly-coding metasurface. The SNR and BER/SER performance is evaluated and verified with simulation. The result indicates that our proposed transmitter design has better communications performance against the existing RIS-based single-carrier modulation transmitters in the Rayleigh channel. Additionally, we propose the RIS-based channel equalization and 1-bit discrete beamforming

method based on perfect CSI for our wideband transmitter. It indicates that the proposed transmitter can adopt multi-antenna techniques when circumventing the need for DSP hardware and costly RF chains. Even without equalization and beamforming, our RIS-based transmitter can have similar communication performance to the conventional transmitter with significantly lower energy consumption. Our RIS-based wideband transmitter provides a promising solution for future wireless wideband communications.

REFERENCES

[1] N. Yu et al., "Light Propagation with Phase Discontinuities: Generalized Laws of Reflection and Refraction," Science, vol. 334, no. 6054, pp. 333–337, Sep. 2011, doi: https://doi.org/10.1126/science.1210713.

[2] W. Tang et al., "Wireless Communications with Programmable Metasurface: New Paradigms, Opportunities, and Challenges on Transceiver Design," IEEE Wireless Communications, vol. 27, no. 2, pp. 180–187, Apr. 2020, doi: https://doi.org/10.1109/MWC.001.1900308.

[3] J. Zhao et al., "Programmable time-domain digital-coding metasurface for non-linear harmonic manipulation and new wireless communication systems," National Science Review, vol. 6, no. 2, pp. 231–238, Nov. 2018, doi: https://doi.org/10.1093/nsr/nwy135.

[4] Jun Yan Dai et al., "Wireless Communication Based on Information Metasurfaces," IEEE Transactions on Microwave Theory and Techniques, vol. 69, no. 3, pp. 1493–1510, Mar. 2021, doi: https://doi.org/10.1109/tmtt.2021.3054662.

[5] W. Tang et al., "Programmable metasurface-based RF chain-free 8PSK wireless transmitter," Electronics Letters, vol. 55, no. 7, pp. 417–420, Apr. 2019, doi: https://doi.org/10.1049/el.2019.0400.

[6] Ming Zheng Chen et al., "Accurate and broadband manipulations of harmonic amplitudes and phases to reach 256 QAM millimeter-wave wireless communications by time-domain digital coding metasurface," National Science Review, vol. 9, no. 1, Jul. 2021, doi: https://doi.org/10.1093/nsr/nwab134.

[7] X. Pi, P. Yi, Z. Xiao, W. Zhang, Z. Han, and X.-G. Xia, "Cost-Efficient RIS-Assisted Transmitter Design With Discrete Phase Shifts for Wireless Communication," IEEE Wireless Communications Letters, vol. 12, no. 3, pp. 520–524, Mar. 2023, doi: https://doi.org/10.1109/lwc.2022.3233023.

[8] C. Huang et al., "Multi-Hop RIS-Empowered Terahertz Communications: A DRL-Based Hybrid Beamforming Design," IEEE Journal on Selected Areas in Communications, vol. 39, no. 6, pp. 1663–1677, Apr. 2021, doi: https://doi.org/10.1109/jsac.2021.3071836.

[9] S. A. Khaleel, E. K. I. Hamad, N. O. Parchin, and M. B. Saleh, "Programmable Beam-Steering Capabilities Based on Graphene Plasmonic THz MIMO Antenna via Reconfigurable Intelligent Surfaces (RIS) for IoT Applications," Electronics, vol. 12, no. 1, p. 164, Dec. 2022, doi: https://doi.org/10.3390/electronics12010164.

[10] Y. Han, L. Xiao, W. Tang, S. Jin, Q. Cheng, and Tie Jun Cui, "Dual-Polarized RIS-Assisted Mobile Communications," IEEE Transactions on Wireless Communications, vol. 21, no. 1, pp. 591–606, Jan. 2022, doi: https://doi.org/10.1109/twc.2021.3098521.

[11] Hai Lin Wang, Yan Kai Zhang, Tai Yi Zhang, H. Feng, and T. Cui, "Broadband and Programmable Amplitude-Phase-Joint-Coding Information Metasurface," ACS Applied Materials Interfaces, vol. 14, no. 25, pp. 29431–29440, Jun. 2022, doi: https://doi.org/10.1021/acsami.2c05907.

[12] J. An, C. Xu, L. Gan, and Lajos Hanzo, "Low-Complexity Channel Estimation and Passive Beamforming for RIS-Assisted MIMO Systems Relying on Discrete Phase Shifts," IEEE Transactions on Communications, vol. 70, no. 2, pp. 1245–1260, Feb. 2022, doi: https://doi.org/10.1109/tcomm.2021.3127924.